MNRAS 000, 1–10 (2022) Preprint 30 November 2022 Compiled using MNRAS LaTeX style file v3.0

Identifying the physical origin of gamma-ray bursts with supervised machine learning

Jia-Wei Luo[1,2⋆], Fei-Fei Wang[3], Jia-Ming Zhu-Ge[4], Ye Li[5], Yuan-Chuan Zou[6] and Bing Zhang[1,2]
[1] *Nevada Center for Astrophysics, University of Nevada, Las Vegas, NV 89154, USA*
[2] *Department of Physics and Astronomy, University of Nevada, Las Vegas, NV 89154, USA*
[3] *School of Mathematics and Physics, Qingdao University of Science and Technology, Qingdao 266061, China*
[4] *Department of Astronomy, University of Science and Technology of China, Hefei 230026, China*
[5] *Purple Mountain Observatory, Chinese Academy of Sciences, Nanjing 100012, China*
[6] *School of Physics, Huazhong University of Science and Technology, Wuhan 430074, China*

Accepted XXX. Received YYY; in original form ZZZ

ABSTRACT

The empirical classification of gamma-ray bursts (GRBs) into long and short GRBs based on their durations is already firmly established. This empirical classification is generally linked to the physical classification of GRBs originating from compact binary mergers and GRBs originating from massive star collapses, or Type I and II GRBs, with the majority of short GRBs belonging to Type I and the majority of long GRBs belonging to Type II. However, there is a significant overlap in the duration distributions of long and short GRBs. Furthermore, some intermingled GRBs, i.e., short-duration Type II and long-duration Type I GRBs, have been reported. A multi-wavelength, multi-parameter classification scheme of GRBs is evidently needed. In this paper, we seek to build such a classification scheme with supervised machine learning methods, chiefly XGBoost. We utilize the GRB Big Table and Greiner's GRB catalog and divide the input features into three subgroups: prompt emission, afterglow, and host galaxy. We find that the prompt emission subgroup performs the best in distinguishing between Type I and II GRBs. We also find the most important distinguishing feature in prompt emission to be T_{90}, hardness ratio, and fluence. After building the machine learning model, we apply it to the currently unclassified GRBs to predict their probabilities of being either GRB class, and we assign the most probable class of each GRB to be its possible physical class.

Key words: (transients:) gamma-ray bursts – methods: data analysis

1 INTRODUCTION

Dating from the early days of Gamma-ray burst (GRB) study, a clear bimodal distribution had been identified in their durations (Kouveliotou et al. 1993). Two classes of GRBs are then proposed based on their durations, namely long GRBs (LGRBs) and short GRBs (SGRBs). The commonly used criterion is based on T_{90}, the time within which 90% of the fluence of the GRB is observed, with the dividing point set to be $T_{90} = 2\,\mathrm{s}$.

LGRBs are thought to be produced by the core-collapse of massive stars (Woosley 1993), and this theory was subsequently supported by direct observational evidence of the association of some LGRBs with Type Ic supernovae (Galama et al. 1998; Woosley & Bloom 2006). SGRBs are thought to be originated from compact star mergers (Eichler et al. 1989), and this theory was supported by the multi-messenger observations of the binary neutron star merger event GW170817/GRB 170817A (Abbott et al. 2017a,b,c; Goldstein et al. 2017; Zhang et al. 2018).

However, this dichotomy is far from perfect. Significant overlap presents in the duration distributions of long and short GRBs, and the duration itself is dependent on the energy band in which it is measured (Mukherjee et al. 1998; Hakkila et al. 2003; Horváth et al. 2006; Zhang & Choi 2008; Veres et al. 2010; Qin et al. 2012; Bromberg et al. 2013; Zhang et al. 2016). Moreover, there are some short-duration GRBs thought to be possibly produced by core-collapse massive stars (Greiner et al. 2009; Tanvir et al. 2009; Salvaterra et al. 2009; Antonelli et al. 2009; Zhang et al. 2009; Guelbenzu et al. 2011; Zhang et al. 2020, 2021; Ahumada et al. 2021), as well as some long-duration GRBs thought to be possibly originated from compact star mergers (Gal-Yam et al. 2006; Gehrels et al. 2006; Fynbo et al. 2006; Della Valle et al. 2006; Zhang et al. 2007; Yang et al. 2022a; Troja et al. 2022; Zhang et al. 2022a).

The existence of these "intermingled" GRBs challenges the practice of classifying GRBs solely based on duration, as well as the names of "long" and "short" GRBs. It is then apparent that more sophisticated classification criteria involving multiple observational parameters are needed. Throughout this study, we refer to the GRB classes based on their physical

⋆ luoj7@unlv.nevada.edu

origins, namely Type I for compact merger GRBs, and Type II for collapsar GRBs, following the classification scheme of Zhang (2006); Zhang et al. (2009). Many other schemes for GRB classification have also been put forward (e.g. Zhang et al. 2009; Lü et al. 2010; Zhang et al. 2012; Bromberg et al. 2013; Lü et al. 2014; Yang et al. 2016; Li et al. 2016; Kulkarni & Desai 2017; Li et al. 2020; Minaev & Pozanenko 2020), yet the classification of long and short GRBs is still largely based on community consensus, and there is a lack of objective classification models with minimal human interference.

In this case, machine learning comes in handy. Capable of automatically generating results without human input after training, machine learning can help us to fathom the differences between Type I and II GRBs, as well as aid us in the classification of newly discovered GRBs. Machine learning have already been widely adopted in the study of GRBs (e.g. Horváth et al. 2006; Řípa et al. 2012; Tarnopolski 2015; Modak et al. 2018; Horváth et al. 2019; Jespersen et al. 2020; Salmon et al. 2022a; Modak 2021; Salmon et al. 2022b; Tarnopolski 2022; Bhave et al. 2022). However, the abovementioned studies predominantly use machine learning methods of the unsupervised type, where only the observed features of the GRBs are inputted into the models, but not the labels (the GRBs' physical classes being Type I or II). On the other hand, the other type of machine learning methods, supervised methods, are also commonly employed by astronomy researchers in the classification of other astronomical objects (e.g. Connor & van Leeuwen 2018; Villa-Ortega et al. 2022; Butter et al. 2022; de Beurs et al. 2022; Yang et al. 2022b; Coronado-Blázquez 2022; Kaur et al. 2022; Fan et al. 2022; Luo et al. 2022b; Zhu-Ge et al. 2022), study on the application of supervised methods on GRB is scarce. Since supervised methods take both features and labels as input, and can produce deterministic predictions of the class of new GRBs, they can be helpful in identifying the true physical origin of intermingled GRBs.

In this study, we apply supervised machine learning methods to the classification of Type I and II GRBs. In Section 2, we introduce the GRB catalogs we utilize and the machine learning methods we use. In Section 3, we present the classification results and feature importance from the machine learning models. In Section 4, we attempt to predict the classes of the unclassified GRBs. Finally, in Section 5, we put forward our conclusions.

2 DATA AND METHODS

We use an updated version of the GRB Big Table (Wang et al. (2020), Wang et al. (in prep)), which contains 7179 GRBs ranging from 1991 April 21 – 2021 July 08. Greiner's GRB catalog (`https://www.mpe.mpg.de/~jcg/grbgen.html`), on the other hand, has 2261 GRBs in the same time range. We match the two catalogs, requiring T_{90} of the selected GRBs in the Big Table to be known, and we label the GRBs based on their labels in Greiner's catalog. GRBs with 'S' at the end of their names are marked as Type I GRBs, while the others are marked as Type II GRBs. We also adopt the consensus classification of some intermingled GRBs: Type II GRB 090426 (Antonelli et al. 2009; Guelbenzu et al. 2011), Type I GRB 060505 (Fynbo et al. 2006) and Type I GRB 060614 (Fynbo et al. 2006; Gal-Yam et al. 2006; Gehrels et al. 2006; Zhang et al. 2007). This leaves us with 144 Type I and 1761 Type II GRBs. We acknowledge that this matching method substantially reduces the size of our sample, but the unmatched GRBs do not have many known features, to begin with. Therefore, we did not discard too much information.

In this study, we pay special interest to the intermingled GRBs. We define intermingled GRBs as GRBs classified as Type I in Greiner's catalog, but have T_{90} values $> 2\,\mathrm{s}$ in the Big Table, or GRBs classified as Type II in Greiner's catalog, but have $T_{90} < 2\,\mathrm{s}$. There are 21 intermingled Type I GRBs and 59 intermingled Type II GRBs in our sample.

We then divide the features in the Big Tables into three subgroups: prompt emission, afterglow and host galaxy. Three subsamples are subsequently created by requiring each GRB in the subsamples to have at least one feature other than T_{90} in the corresponding feature group to be known. We also divide each subsample into training sets and test sets with a 7:3 ratio, while keeping the ratio of Type I to Type II GRBs the same in the training sets and test sets. The training sets are used to train the machine learning model, while the test sets are used to test the performance of the model after it is trained.

While it is common practice to impute the missing values in the data with some type of algorithm, we find that imputation introduces false information in the feature importance we later calculate, which is also suggested by some other studies (e.g. Seijo-Pardo et al. 2019; Yu et al. 2022). Since the `XGBoost` classifier (Chen & Guestrin 2016) can automatically handle missing values, we simply input our data without imputation.

Then, we note that the Type I and Type II GRBs in our sample are significantly imbalanced by a ratio of $\sim 1:10$. Because this apparent ratio could be caused by selection effects, we should not introduce this ratio to our training data. However, the commonly used synthetic minority over-sampling technique (SMOTE) (Chawla et al. 2002) cannot be applied to data with missing values. Instead, we assign different sample weights for the two classes calculated with `scikit-learn` (Pedregosa et al. 2011).

Finally, we input the training sets into the `XGBoost` classifier to train the machine learning model. After training, we use the test set and the commonly used F_1 score (van Rijsbergen 1979; Sasaki 2007) to assess the performance of our models. A more intuitive metric, accuracy, is disfavored here because our data is imbalanced. A model simply predicts all GRBs as Type II can still score 92% accuracy.

To test which input feature has the best capability in distinguishing between Type I and II GRBs, we adopt permutation feature importance (Breiman 2001; Altmann et al. 2010; Fisher et al. 2019) on the entire dataset. Each time we randomly shuffle the values of one input feature across all data points, thus removing the correlation between this feature and the output label. We observe the drop in F_1 score and use it as the importance of the feature. We repeat this process 100 times for each feature and take the average from the trials as the final feature importance. We also draw the error bars with standard deviations from the trials.

Feature name	Unit	Description	Log
`T90`	s	Time within which 90% of the fluence of the GRB is observed	Y
`variability1`	—	Variability, based on the Fenimore & Ramirez-Ruiz (2000) definition	N
`F_g`	10^{-6} erg cm^{-2}	Fluence in the 20–2000 keV energy band	Y
`HR`	—	Hardness ratio between 100–2000 keV and 20–100 keV	Y
`F_pk1`	10^{-6} erg cm^{-2} s^{-1}	Peak flux in the 1 s time bin in the rest-frame 1–10 × 10^4 keV energy band	Y
`P_pk4`	photon cm^{-2} s^{-1}	Peak photon flux in the 1 s time bin of 10–1000 keV	Y
`alpha_band`	—	Low-energy spectrum index of the Band model	N
`beta_band`	—	High-energy spectrum index of the Band model	N
`E_P_band`	keV	Spectral peak energy of the Band model	Y
`alpha_cpl`	—	Spectrum index of the cutoff power-law (CPL) model	N
`E_P_cpl`	keV	Spectral peak energy of the cutoff power-law (CPL) model	Y
`alpha_spl`	—	Spectrum index of the simple power-law (SPL) model	N
`spectral_lag`	ms MeV^{-1}	Spectral time lag	N
`z`	—	Redshift	N
`D_L`	10^{28} cm	Luminosity distance	Y
`E_iso`	10^{52} erg	Isotropic gamma-ray energy in the rest-frame 1–10 × 10^4 keV energy band	Y
`L_pk`	10^{52} erg s^{-1}	Isotropic peak luminosity in the 1 s time bin in the rest-frame 1–10 × 10^4 keV energy band	Y

Table 1. List of features used in the prompt emission subgroup. For features with multiple definitions (e.g., variability, F_pk), we choose the one with the most known data. Directly measured features are listed above the horizontal line, while the derived features are listed below the line.

Feature name	Unit	Description	Log
`theta_j`	rad	Jet-opening angle	Y
`Gamma0`	—	Initial Lorentz factor	Y
`log_t_burst`	s	Duration of the GRB central engine	Y
`t_b`	d	Jet break time	Y
`t_pkX`	s	Peak flux time in the X-ray band	Y
`t_pkOpte`	s	Peak of the early optical afterglow light curve	Y
`t_pkOpt`	s	Peak flux time in the optical band	Y
`F_X11hr`	Jy	Flux density in the X-ray band 11 h after the trigger time of the burst	Y
`beta_X11hr`	—	Index in X-ray band 11 h after the trigger time of the burst	N
`F_Opt11hr`	Jy	Flux density in the optical band 11 h after the trigger time of the burst	Y
`t_radio_pk`	s	Peak radio time in the afterglow	Y
`F_radio_pk`	Jy	Peak flux density in the radio band at 8.46 GHz	Y
`T_ai`	s	Rest-frame time at the end of the plateau phase in log in X-ray	Y
`L_a`	erg s^{-1}	Isotropic X-ray luminosity at the time Ta	Y

Table 2. List of features used in the afterglow subgroup.

Feature name	Unit	Description	Log
`offset`	kpc	Distance from the burst location to the center of the host galaxy	Y
`metallicity`	—	Metallicity of the host; the value is 12 + log[O/H]	N
`Mag`	magnitude	Absolute magnitude in the 3.6 um rest wavelength	N
`N_H`	10^{21} cm^{-2}	Column density of hydrogen	Y
`A_V`	—	Dust extinction	N
`SFR`	$M_\odot$ yr^{-1}	Star formation rate	Y
`SSFR`	Gyr^{-1}	Specific star formation rate	Y
`Age`	Myr	The age of the GRB host galaxy	Y
`Mass`	$M_\odot$	Stellar mass	Y

Table 3. List of features used in the host galaxy subgroup.

3 RESULTS

3.1 Prompt emission

Many studies suggested adding hardness ratio (HR) to the T_{90} classification criterion to form a two-dimensional criteria will yield better results (e.g. Horváth et al. 2006, 2010; Řípa et al. 2012; Zhang et al. 2012; Bhat et al. 2016; Yang et al. 2016; Horváth et al. 2018; Tarnopolski 2019; Zhang et al. 2022b). Similarly, the power-law index or peak energy E_p of the spectrum of prompt emission can also take the place of hardness ratio (Zhang et al. 2012; Goldstein et al. 2010; Nava et al. 2011). In general, Type I GRBs have harder spectra compared with Type II GRBs. Goldstein et al. (2010) further proposes classification on the E_p – fluence plane. Since fluence is highly related to duration, this scheme also follows the HR - T_{90} scheme.

Some other studies (e.g. Zhang et al. 2009, 2012; Qin & Chen 2013; Tsutsui et al. 2013; Minaev & Pozanenko 2020) suggest that the famous Amati relation (Amati et al. 2002, 2009; Kumar & Zhang 2015) of the peak energy E_p and the isotropic energy E_{iso} of GRB prompt emission are different for Type I and II GRBs, and thus the $E_p - E_{iso}$ plane can be used to distinguish between Type I and II GRBs.

In addition, Norris & Bonnell (2006); Yi et al. (2006); Gehrels et al. (2006); Zhang (2006); Ukwatta et al. (2010); Minaev et al. (2014); Bernardini et al. (2015); Shao et al. (2017) propose to classify Type I and II GRBs based on spectral lag τ and the τ – peak luminosity L_p plane, where Type I GRBs have smaller spectral lags and peak luminosities.

Association with supernovae (SN) is also a very important distinguishing factor between Type I and II GRBs, as SN associations provide smoking-gun evidence of the GRB progenitor. However, the Big Table only contains SN association information for 22 GRBs. For those GRBs without SN association information, it is unknown whether there truly was no SN associated with the GRB, or there simply was no observation, or most likely, there was an optical observation, but the SN was outshone by the bright optical afterglow. We find that including SN association makes our results worse, therefore we do not include SN in our models.

With the prompt emission subgroup, we are able to obtain a F_1 score of 0.7838 on the test set, and 0.5882 on the intermingled GRBs. The corresponding confusion matrices and feature importance are shown in Figure 1. Our model can predict most GRBs correctly based on prompt emission data, and T_{90} is the most prominent feature, with feature importance much higher than other features.

However, when we remove T_{90} from the prompt emission subgroup and carry out the same analysis, while we get a lower F_1 score of 0.6667 on the test set as expected, but we also get a higher F_1 score of 0.8966 on the intermingled GRBs. The corresponding confusion matrices and feature importance are shown in Figure 2. This shows that T_{90} can be misleading to the machine learning model for intermingled GRBs, and multiple observational parameters are needed for more accurate classification of GRBs.

We also find the fluence `F_g` and hardness ratio `HR` to be the most important feature after T_{90}. Since fluence is directly related to the duration, our results confirm the finding of other studies.

In order to measure the importance of other features, we further exclude fluence and hardness ratio from our feature group, and carry out the same machine learning analysis. We obtain F_1 score of 0.5758 on the test set and 0.7333 on the intermingled GRBs. The corresponding confusion matrices and feature importance are shown in Figure 3. While the general F_1 score drops again, the F_1 score for intermingled sample remains high. The most important features are again related to the spectral shape, such as `E_iso`, `alpha_cpl`, `E_p_cpl` and `alpha_spl`. The flux-related feature of `F_pk1` and `P_pk4` are also important, as well as spectral lag.

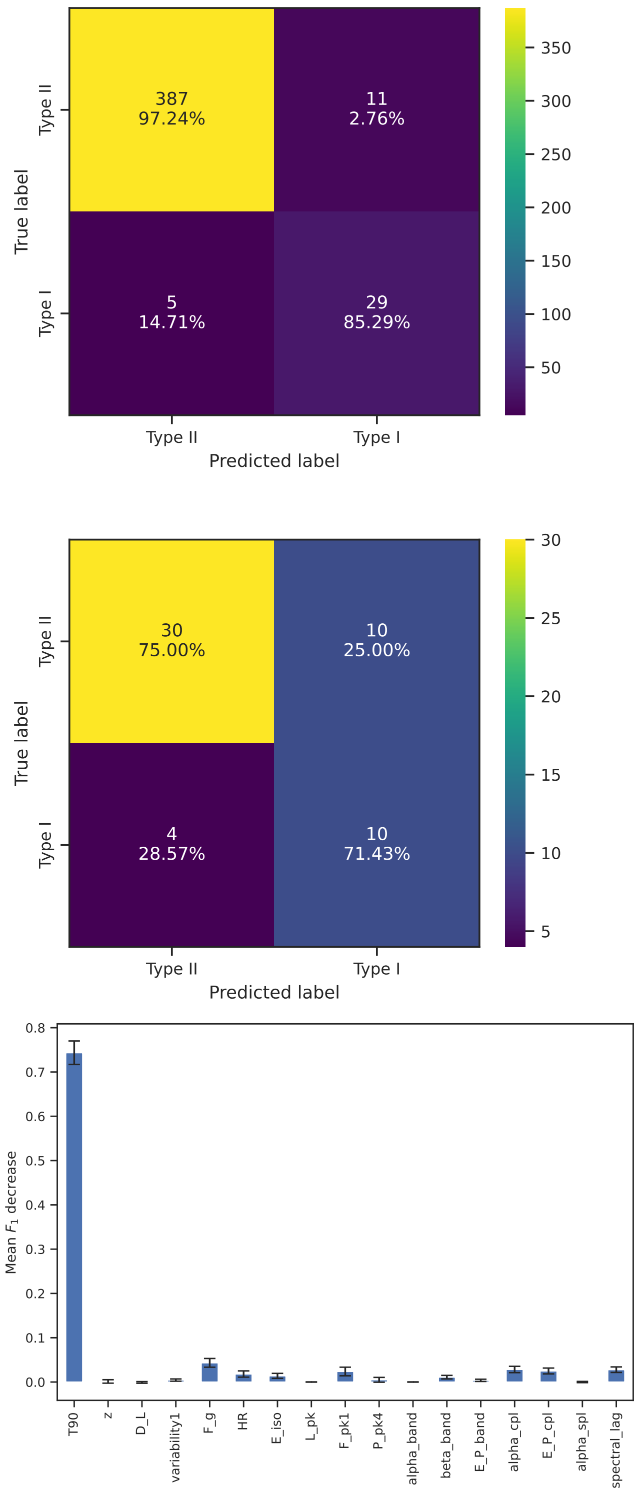

Figure 1. Example of confusion matrices and feature importance for the prompt emission subgroup. Upper: Confusion matrix on the entire test set; Middle: Confusion matrix on the intermingled GRBs; Lower: Feature importance on the entire dataset.

3.2 Afterglow

Gehrels et al. (2008); Nysewander et al. (2009); D'Avanzo et al. (2012); Margutti et al. (2013) pointed out that afterglows of Type I GRBs mostly have lower X-ray luminosity and energy and decay faster. There are also correlations among afterglow X-ray energy, X-ray afterglow luminosity, prompt emission isotropic energy E_{iso}, peak luminosity L_p and peak energy E_p. Combined with the findings mentioned

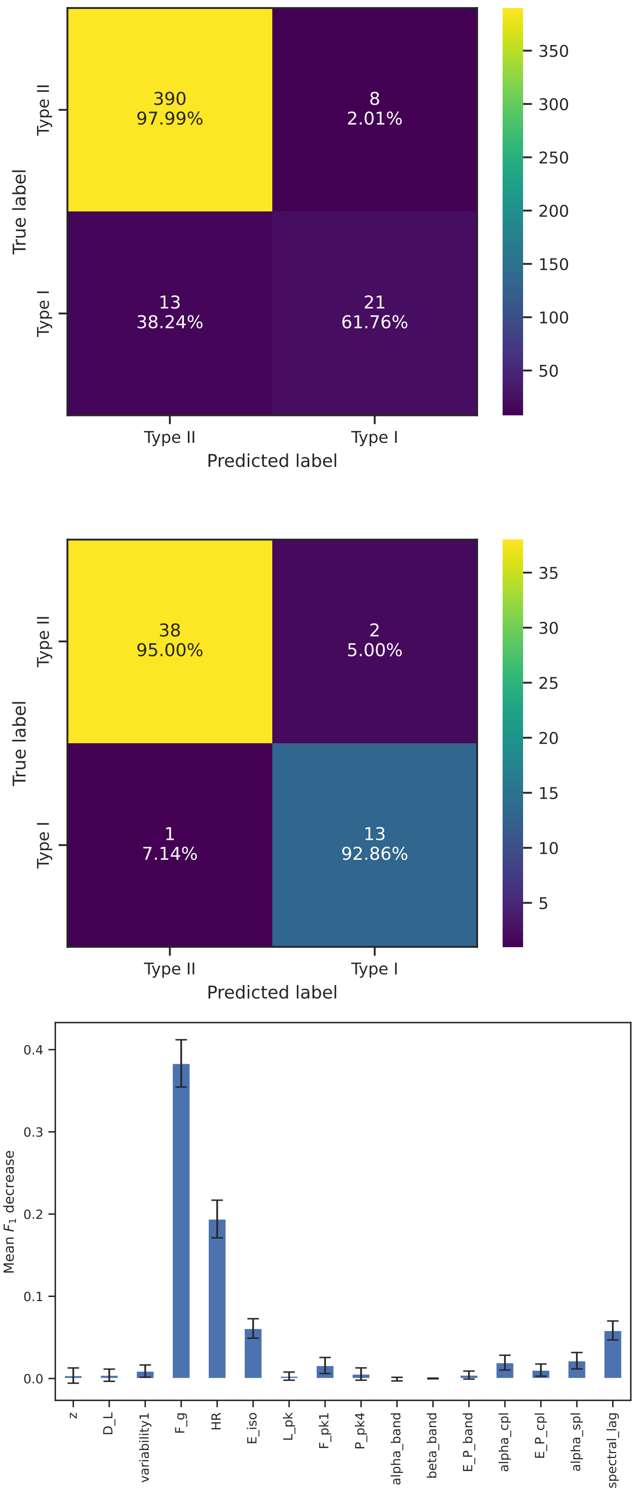

Figure 2. Example of confusion matrices and feature importance for the prompt emission subgroup without T_{90}. Upper: Confusion matrix on the entire test set; Middle: Confusion matrix on the intermingled GRBs; Lower: Feature importance on the entire dataset.

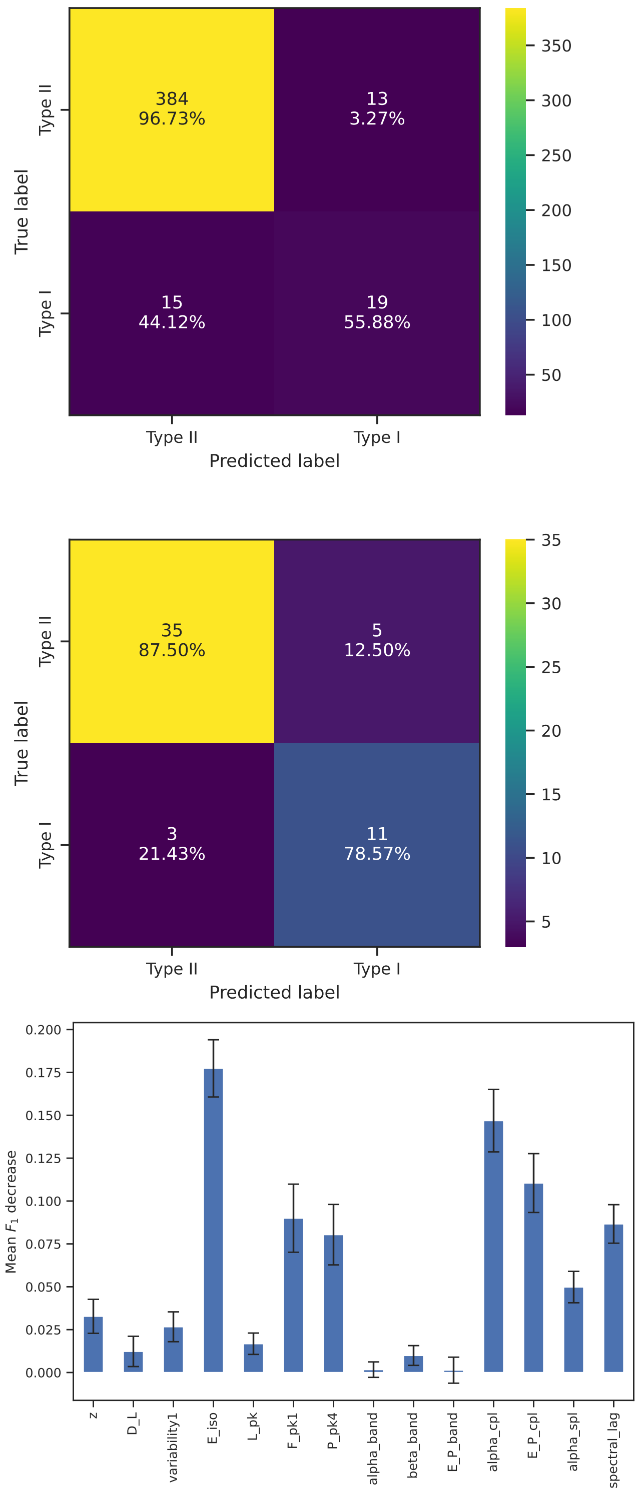

Figure 3. Example of confusion matrices and feature importance for the prompt emission subgroup without T_{90}, F_g or HR. Upper: Confusion matrix on the entire test set; Middle: Confusion matrix on the intermingled GRBs; Lower: Feature importance on the entire dataset.

in Section 3.1, X-ray afterglow luminosity can also be employed for GRB classification.

Kann et al. (2011) found that similar to X-ray, optical afterglows of Type I GRBs are significantly fainter than that of Type II GRBs, and similar afterglow-prompt emission correlations also exist in the optical band.

With the afterglow subgroup, we are able to obtain F_1 score of 0.4444 on the test set and 0.875 on the intermingled GRBs. The corresponding confusion matrices and feature importance are shown in Figure 4. We found the most important feature to be 11-hour beta index in X-ray. 11-hour fluxes of X-ray and optical are also important. In general, we find that afterglow features perform poorly in GRB classification.

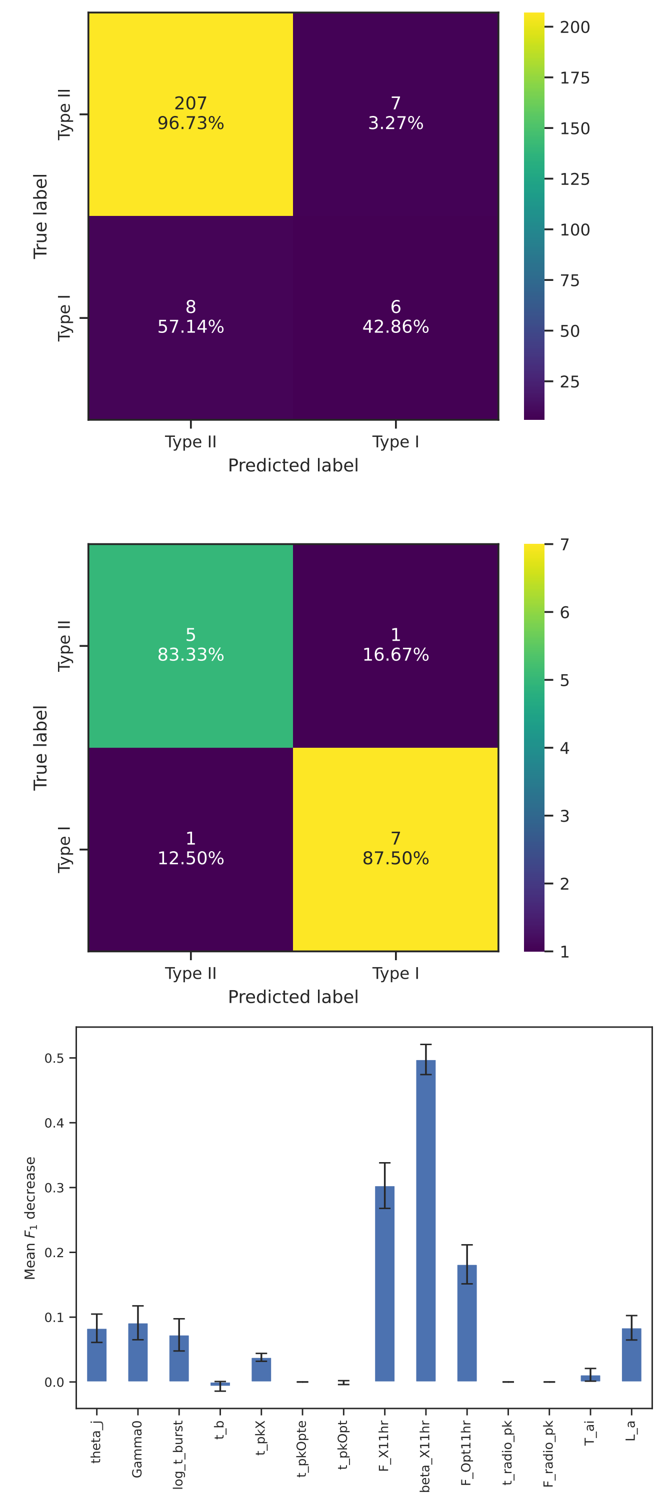

Figure 4. Example of confusion matrices and feature importance for the afterglow subgroup. Upper: Confusion matrix on the entire test set; Middle: Confusion matrix on the intermingled GRBs; Lower: Feature importance on the entire dataset.

3.3 Host galaxy

The different progenitors of Type I and II GRBs also have a substantial impact on the properties of their host galaxies. The short lifetime of Type II GRB progenitors (Woosley et al. 2002) makes their event rate to generally follow the star formation rate (SFR) of the host galaxies, and Type II GRB host galaxies generally have higher SFR. (Bloom et al. 2002; Chary et al. 2007; Savaglio et al. 2009; Levesque et al. 2010a; Robertson & Ellis 2011; Levesque 2014; Wei et al. 2014; Trenti et al. 2015; Cucchiara et al. 2015; Lan et al. 2022). The redshift distribution of Type I GRBs are found to be delayed with respect to the star formation history, and thus host galaxies of Type I GRBs generally have lower SFR respectively (Piran 1992; Nakar et al. 2006; Zheng & Ramirez-Ruiz 2007; Virgili et al. 2011; Wanderman & Piran 2015; Luo et al. 2022a).

Type II GRB hosts also have low metallicity, which is required to form high-mass progenitors. (Fynbo et al. 2003; Prochaska et al. 2004; Fruchter et al. 2006; Levesque et al. 2010b; Kocevski & West 2011; Mannucci et al. 2011; Campisi et al. 2011; Graham & Fruchter 2017). Type I GRB hosts, on the other hand, are found to have higher metallicity (e.g. Berger 2014).

Type II GRBs usually occur in regions with active star formation and are, therefore, closer to the center of the galaxy and in brighter regions. Type I GRBs, however, have larger offsets from the galactic center as the evolution of compact binary mergers require supernova events that “kick off” the binary system away from the location where they are formed (Bloom et al. 2002; Fruchter et al. 2006; Fong et al. 2013; Blanchard et al. 2016; Wang et al. 2018; Li et al. 2020; O’Connor et al. 2022; Fong et al. 2022).

With the afterglow subgroup, we are able to obtain F_1 score of 0.64 on the test set and 0.9231 on the intermingled GRBs. The corresponding confusion matrices and feature importance are shown in Figure 5. We found the most important feature to be offset.

In order to find other important features, we also carry out the same analysis on the host galaxy subgroup without offset. We get F_1 score of 0.5714 on the test set and 0.8889 on the intermingled GRBs with the host galaxy subgroup without offset. The corresponding confusion matrices and feature importance are shown in Figure 6. Age, `A_V` and stellar mass are also fairly important. One caveat here is that none of the Type I GRBs have information of `Mag` and `N_H`. Thus, more data is needed to measure the importance of these features in distinguishing Type I and II GRBs.

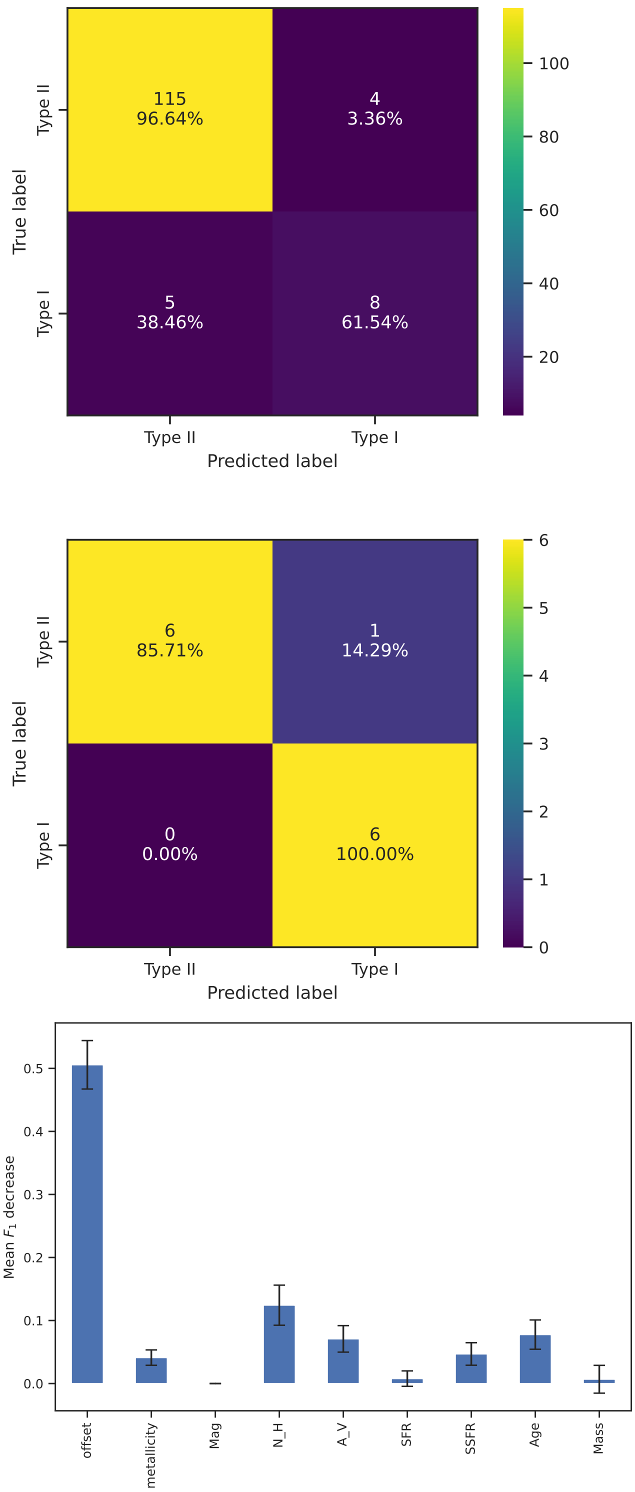

Figure 5. Example of confusion matrices and feature importance for the host galaxy subgroup. Upper: Confusion matrix on the entire test set; Middle: Confusion matrix on the intermingled GRBs; Lower: Feature importance on the entire dataset.

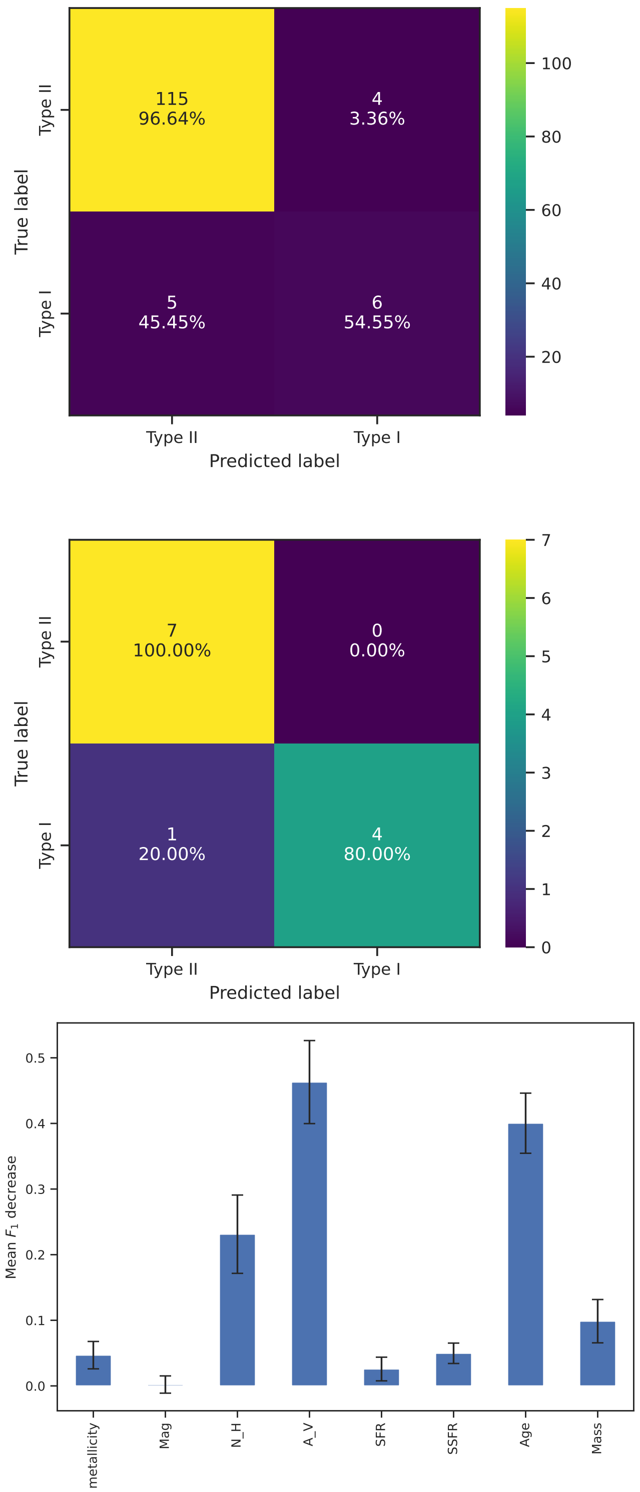

Figure 6. Example of confusion matrices and feature importance for the host galaxy subgroup without offset. Upper: Confusion matrix on the entire test set; Middle: Confusion matrix on the intermingled GRBs; Lower: Feature importance on the entire dataset.

3.4 Comparing the feature subgroups

Because the training and test set splitting process introduces randomness to the results, F_1 scores from a single trial may not be able to fully reflect the abilities in distinguishing Type I and II GRBs for different feature subgroups. Therefore, we repeat the random splitting and training process 1000 times, and record the F_1 scores of each feature subgroup on the entire test set and intermingled GRBs.

We report the average F_1 scores, along with standard deviations based on the 1000 trials for each feature subgroup on the entire test set and intermingled GRBs in Table 4. We found that the prompt emission subgroup performs the best in predicting Type I and II GRBs, while the average F_1 score of the afterglow subgroup is significantly lower. Host galaxy comes in between the two subgroups. However, prompt emission including T_{90} performs the worst on the intermingled GRBs.

4 PREDICTING UNCLASSIFIED GRBS

After building the models, we then move on to predict the classes of the unclassified GRBs in the Big Table. Since nearly all unclassified GRBs do not have afterglow and host galaxy features measured, we only use the prompt emission features in this section. We also add `T_90`, `F_pk2` (peak flux in the 64 ms bin) and `P_pk1` (peak photon flux in the 64 ms bin) to increase the information available to the machine learning model.

We train the model using the same method described in Section 2 with all the classified GRBs with at least one feature we intend to use and T_{90} known, and use the trained model to predict the probabilities of the unclassified GRBs being either class. We also require the unclassified GRBs to have at least one feature and T_{90} known. 1533 GRBs are used for training, and the class probabilities of 3225 unclassified GRBs are predicted. For each unclassified GRB, the class in which they are predicted with the highest probability is assigned as their class. 2502 GRBs are predicted as Type II, while 723 GRBs are predicted as Type I. The prediction results are listed in Table 5. We also graph the probability distribution of the unclassified GRBs being Type II in Figure 7.

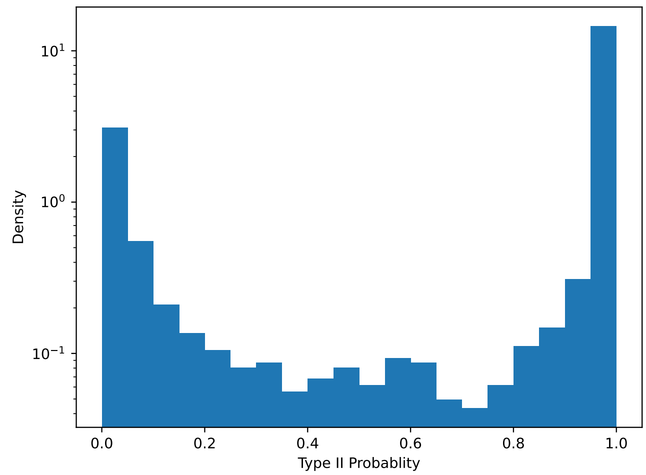

Figure 7. Probability distribution of the unclassified GRBs being Type II. The probability for Type I is 1 − the shown value.

5 CONCLUSIONS

In this paper, we applied supervised machine methods, mainly `XGBoost`, to the classification of Type I and II GRBs. We come up with the following conclusions:

- Classifying GRBs solely based on T_{90} can yield unsatisfactory results, especially on intermingled GRBs. Criteria based on multiple observational parameters are needed.
- Machine learning method can effectively classify GRBs, even intermingled ones.
- The fact that supervised learning with two classes of GRBs can effectively classify intermingled GRBs indirectly rejects the existence of a third intermediate GRB class proposed based on duration distribution.
- We found that the best feature group in predicting Type I or II GRB is prompt emission. Among features on prompt emission, we found that T_{90} still separates Type I and II GRBs the best. Besides T_{90}, fluence and hardness ratio are also important features. Since fluence is correlated with T_{90}, this is consistent with the traditional way of classifying GRBs on the T_{90} – HR plane.
- We predict the class of some of the GRBs not present in Greiner's catalog. Their predicted class and their probabilities of being either are shown in Table 5.

6 ACKNOWLEDGEMENTS

This work is partially supported by the Top Tier Doctoral Graduate Research Assistantship (TTDGRA) and Nevada Center for Astrophysics at the University of Nevada, Las Vegas.

DATA AVAILABILITY

The GRB Big Table by Wang et al. (2020) is available at https://cdsarc.cds.unistra.fr/viz-bin/cat/J/ApJ/893/77. The updated version used in this study will be published along with a separate paper. Greiner's GRB catalog is available at https://www.mpe.mpg.de/~jcg/grbgen.html. The code used in this paper can be shared upon request to the authors.

REFERENCES

Abbott B. P., et al., 2017a, Phys. Rev. Lett., 119, 161101
Abbott B. P., et al., 2017b, ApJ, 848, L12
Abbott B. P., et al., 2017c, ApJ, 848, L13
Ahumada T., et al., 2021, Nature Astronomy, 5, 917
Altmann A., Toloşi L., Sander O., Lengauer T., 2010, Bioinformatics, 26, 1340
Amati L., et al., 2002, A&A, 390, 81
Amati L., Frontera F., Guidorzi C., 2009, A&A, 508, 173
Antonelli L. A., et al., 2009, A&A, 507, L45
Berger E., 2014, ARA&A, 52, 43
Bernardini M. G., et al., 2015, MNRAS, 446, 1129
Bhat P. N., et al., 2016, ApJS, 223, 28

Feature subgroup	F_1 Mean	F_1 SD	Intermingled F_1 Mean	Intermingled F_1 SD
Prompt emission	0.7586	0.0471	0.6342	0.0926
Prompt emission, without `T90`	0.6732	0.0585	0.7594	0.0761
Prompt emission, without `T90`, `HR`, `F_g`	0.5198	0.0646	0.7810	0.0797
Afterglow	0.4349	0.1019	0.7976	0.1028
Host galaxy	0.6662	0.0818	0.9147	0.0797
Host galaxy, without `offset`	0.5261	0.1035	0.7962	0.1414

Table 4. List of average F_1 scores and standard deviations obtained with different feature subgroups.

GRB	$p_{\rm I}$	$p_{\rm II}$	Type
180505A	0.001	0.999	II
180416B	0.001	0.999	II
180416A	0.003	0.997	II
180218A	0.001	0.999	II
180126A	0.003	0.997	II
180120A	0.001	0.999	II
171230B	0.002	0.998	II
171230A	0.003	0.997	II
171227	0.001	0.999	II
171223A	0.633	0.367	I

Table 5. Prediction results of the unclassified FRBs. The probability of them being Type I or II are shown as $p_{\rm I}$ and $p_{\rm II}$ respectively. This is an example of the first ten rows of the table. The full version is available in the online version of this paper as supplementary material.

Bhave A., Kulkarni S., Desai S., Srijith P. K., 2022, Ap&SS, 367, 39

Blanchard P. K., Berger E., Fong W.-f., 2016, ApJ, 817, 144

Bloom J. S., Kulkarni S. R., Djorgovski S. G., 2002, AJ, 123, 1111

Breiman L., 2001, Machine Learning, 45, 5

Bromberg O., Nakar E., Piran T., Sari R., 2013, ApJ, 764, 179

Butter A., Finke T., Keil F., Krämer M., Manconi S., 2022, J. Cosmology Astropart. Phys., 2022, 023

Campisi M. A., Tapparello C., Salvaterra R., Mannucci F., Colpi M., 2011, MNRAS, 417, 1013

Chary R., Berger E., Cowie L., 2007, ApJ, 671, 272

Chawla N. V., Bowyer K. W., Hall L. O., Kegelmeyer W. P., 2002, Journal of Artificial Intelligence Research, 16, 321

Chen T., Guestrin C., 2016, in Proceedings of the 22nd ACM SIGKDD International Conference on Knowledge Discovery and Data Mining. pp 785–794 (arXiv:1603.02754), doi:10.1145/2939672.2939785, http://arxiv.org/abs/1603.02754

Connor L., van Leeuwen J., 2018, AJ, 156, 256

Coronado-Blázquez J., 2022, MNRAS, 515, 1807

Cucchiara A., Fumagalli M., Rafelski M., Kocevski D., Prochaska J. X., Cooke R. J., Becker G. D., 2015, ApJ, 804, 51

D'Avanzo P., et al., 2012, MNRAS, 425, 506

Della Valle M., et al., 2006, Nature, 444, 1050

Eichler D., Liviot M., Piran T., Schramm D. N., 1989, Nature, p. 3

Fan J.-H., et al., 2022, Universe, 8, 436

Fenimore E. E., Ramirez-Ruiz E., 2000, Redshifts For 220 BATSE Gamma-Ray Bursts Determined by Variability and the Cosmological Consequences (arXiv:astro-ph/0004176), doi:10.48550/arXiv.astro-ph/0004176, http://arxiv.org/abs/astro-ph/0004176

Fisher A., Rudin C., Dominici F., 2019, Journal of Machine Learning Research, 20, 1

Fong W., et al., 2013, ApJ, 769, 56

Fong W.-f., et al., 2022, Short GRB Host Galaxies I: Photometric and Spectroscopic Catalogs, Host Associations, and Galactocentric Offsets (arXiv:2206.01763), http://arxiv.org/abs/2206.01763

Fruchter A. S., et al., 2006, Nature, 441, 463

Fynbo J. P. U., et al., 2003, Astronomy & Astrophysics, 406, L63

Fynbo J. P. U., et al., 2006, Nature, 444, 1047

Gal-Yam A., et al., 2006, Nature, 444, 1053

Galama T. J., et al., 1998, Nature, 395, 670

Gehrels N., et al., 2006, Nature, 444, 1044

Gehrels N., et al., 2008, ApJ, 689, 1161

Goldstein A., Preece R. D., Briggs M. S., 2010, ApJ, 721, 1329

Goldstein A., et al., 2017, ApJ, 848, L14

Graham J. F., Fruchter A. S., 2017, ApJ, 834, 170

Greiner J., et al., 2009, ApJ, 693, 1610

Guelbenzu A. N., et al., 2011, A&A, 531, L6

Hakkila J., Giblin T. W., Roiger R. J., Haglin D. J., Paciesas W. S., Meegan C. A., 2003, ApJ, 582, 320

Horváth I., Balázs L. G., Bagoly Z., Ryde F., Mészáros A., 2006, Astronomy & Astrophysics, 447, 23

Horváth I., Bagoly Z., Balázs L. G., Postigo A. d. U., Veres P., Mészáros A., 2010, ApJ, 713, 552

Horváth I., Tóth B. G., Hakkila J., Tóth L. V., Balázs L. G., Rácz I. I., Pintér S., Bagoly Z., 2018, Ap&SS, 363, 53

Horváth I., Hakkila J., Bagoly Z., Tóth L. V., Rácz I. I., Pintér S., Tóth B. G., 2019, Ap&SS, 364, 105

Jespersen C. K., Severin J. B., Steinhardt C. L., Vinther J., Fynbo J. P. U., Selsing J., Watson D., 2020, ApJ, 896, L20

Kann D. A., et al., 2011, ApJ, 734, 96

Kaur A., Kerby S., Falcone A. D., 2022, Using Neural Networks to Differentiate Newly Discovered BL Lacs and FSRQs among the 4FGL Unassociated Sources Employing Gamma-ray, X-ray, UV/Optical and IR Data (arXiv:2208.10015), http://arxiv.org/abs/2208.10015

Kocevski D., West A. A., 2011, ApJ, 735, L8

Kouveliotou C., Meegan C. A., Fishman G. J., Bhat N. P., Briggs M. S., Koshut T. M., Paciesas W. S., Pendleton G. N., 1993, ApJ, 413, L101

Kulkarni S., Desai S., 2017, Ap&SS, 362, 70

Kumar P., Zhang B., 2015, Phys. Rep., 561, 1

Lan G.-X., Wei J.-J., Li Y., Zeng H.-D., Wu X.-F., 2022, ApJ, 938, 129

Levesque E. M., 2014, PASP, 126, 1

Levesque E. M., Berger E., Kewley L. J., Bagley M. M., 2010a, AJ, 139, 694

Levesque E. M., Kewley L. J., Berger E., Zahid H. J., 2010b, AJ, 140, 1557

Li Y., Zhang B., Lü H.-J., 2016, ApJS, 227, 7

Li Y., Zhang B., Yuan Q., 2020, ApJ, 897, 154

Lü H.-J., Liang E.-W., Zhang B.-B., Zhang B., 2010, ApJ, 725, 1965

Lü H.-J., Zhang B., Liang E.-W., Zhang B.-B., Sakamoto T., 2014, MNRAS, 442, 1922

Luo J.-W., Li Y., Ai S., Gao H., Zhang B., 2022a, MNRAS, 516, 1654

Luo J.-W., Zhu-Ge J.-M., Zhang B., 2022b, MNRAS, 518, 1629

Mannucci F., Salvaterra R., Campisi M. A., 2011, MNRAS, 414, 1263

Margutti R., et al., 2013, MNRAS, 428, 729

Minaev P. Y., Pozanenko A. S., 2020, MNRAS, 492, 1919

Minaev P. Y., Pozanenko A. S., Molkov S. V., Grebenev S. A., 2014, Astronomy Letters, 40, 235

Modak S., 2021, Astronomy and Computing, 34, 100441
Modak S., Chattopadhyay A. K., Chattopadhyay T., 2018, Communications in Statistics - Simulation and Computation, 47, 1088
Mukherjee S., Feigelson E. D., Jogesh Babu G., Murtagh F., Fraley C., Raftery A., 1998, ApJ, 508, 314
Nakar E., Gal-Yam A., Fox D. B., 2006, ApJ, 650, 281
Nava L., Ghirlanda G., Ghisellini G., Celotti A., 2011, A&A, 530, A21
Norris J. P., Bonnell J. T., 2006, ApJ, 643, 266
Nysewander M., Fruchter A. S., Pe'er A., 2009, ApJ, 701, 824
O'Connor B., et al., 2022, MNRAS, 515, 4890
Pedregosa F., et al., 2011, The Journal of Machine Learning Research, 12, 2825
Piran T., 1992, ApJ, 389, L45
Prochaska J. X., et al., 2004, ApJ, 611, 200
Qin Y.-P., Chen Z.-F., 2013, MNRAS, 430, 163
Qin Y., et al., 2012, ApJ, 763, 15
Řípa J., Mészáros A., Veres P., Park I. H., 2012, ApJ, 756, 44
Robertson B. E., Ellis R. S., 2011, ApJ, 744, 95
Salmon L., Hanlon L., Martin-Carrillo A., 2022a, Galaxies, 10, 77
Salmon L., Hanlon L., Martin-Carrillo A., 2022b, Galaxies, 10, 78
Salvaterra R., et al., 2009, Nature, 461, 1258
Sasaki Y., 2007, Teach tutor mater, 1, 1
Savaglio S., Glazebrook K., Borgne D. L., 2009, ApJ, 691, 182
Seijo-Pardo B., Alonso-Betanzos A., Bennett K. P., Bolón-Canedo V., Josse J., Saeed M., Guyon I., 2019, Neurocomputing, 342, 97
Shao L., et al., 2017, ApJ, 844, 126
Tanvir N. R., et al., 2009, Nature, 461, 1254
Tarnopolski M., 2015, MNRAS, 454, 1132
Tarnopolski M., 2019, ApJ, 870, 105
Tarnopolski M., 2022, A&A, 657, A13
Trenti M., Perna R., Jimenez R., 2015, ApJ, 802, 103
Troja E., et al., 2022, A Long Gamma-Ray Burst from a Merger of Compact Objects (arXiv:2209.03363), doi:10.48550/arXiv.2209.03363, http://arxiv.org/abs/2209.03363
Tsutsui R., Yonetoku D., Nakamura T., Takahashi K., Morihara Y., 2013, MNRAS, 431, 1398
Ukwatta T. N., et al., 2010, ApJ, 711, 1073
Veres P., Bagoly Z., Horváth I., Mészáros A., Balázs L. G., 2010, ApJ, 725, 1955
Villa-Ortega V., Dent T., Barroso A. C., 2022, Astrophysical Source Classification and Distance Estimation for PyCBC Live (arXiv:2203.10080), http://arxiv.org/abs/2203.10080
Virgili F. J., Zhang B., O'Brien P., Troja E., 2011, ApJ, 727, 109
Wanderman D., Piran T., 2015, MNRAS, 448, 3026
Wang F.-F., Zou Y.-C., Liu Y., Liao B., Moharana R., 2018, Journal of High Energy Astrophysics, 18, 21
Wang F., Zou Y.-C., Liu F., Liao B., Liu Y., Chai Y., Xia L., 2020, ApJ, 893, 77
Wei J.-J., Wu X.-F., Melia F., Wei D.-M., Feng L.-L., 2014, MNRAS, 439, 3329
Woosley S. E., 1993, ApJ, 405, 273
Woosley S. E., Bloom J. S., 2006, ARA&A, 44, 507
Woosley S. E., Heger A., Weaver T. A., 2002, Reviews of Modern Physics, 74, 1015
Yang E. B., Zhang Z. B., Jiang X. X., 2016, Ap&SS, 361, 257
Yang J., et al., 2022a, A Peculiar, Long-Duration Gamma-Ray Burst from a Neutron Star-White Dwarf Merger (arXiv:2204.12771), http://arxiv.org/abs/2204.12771
Yang H., Hare J., Kargaltsev O., Volkov I., Chen S., Rangelov B., 2022b, Classifying Unidentified X-ray Sources in the Chandra Source Catalog Using a Multi-wavelength Machine Learning Approach (arXiv:2206.13656), http://arxiv.org/abs/2206.13656
Yi T., Liang E., Qin Y., Lu R., 2006, MNRAS, 367, 1751
Yu K., Yang Y., Ding W., 2022, ACM Transactions on Knowledge Discovery from Data, 16, 66:1
Zhang B., 2006, Nature, 444, 1010
Zhang Z.-B., Choi C.-S., 2008, Astronomy & Astrophysics, 484, 293
Zhang B., Zhang B.-B., Liang E.-W., Gehrels N., Burrows D. N., Mészáros P., 2007, ApJ, 655, L25
Zhang B., et al., 2009, ApJ, 703, 1696
Zhang F.-W., Shao L., Yan J.-Z., Wei D.-M., 2012, ApJ, 750, 88
Zhang B., Lü H.-J., Liang E.-W., 2016, Space Sci. Rev., 202, 3
Zhang B.-B., et al., 2018, Nature Communications, 9, 447
Zhang B., et al., 2020, Preprint, A Genuinely Short Gamma-Ray Burst from Massive Star Core Collapse, https://www.researchsquare.com/article/rs-131126/v1. In Review, doi:10.21203/rs.3.rs-131126/v1, https://www.researchsquare.com/article/rs-131126/v1
Zhang B.-B., et al., 2021, Nature Astronomy, 5, 911
Zhang B., et al., 2022a, Preprint, A Long-Duration Gamma-Ray Burst with a Peculiar Origin, https://www.researchsquare.com/article/rs-1634483/v1. In Review, doi:10.21203/rs.3.rs-1634483/v1, https://www.researchsquare.com/article/rs-1634483/v1
Zhang L., Luo J.-J., Huang Y.-F., Gong Y.-J., Wu S., 2022b, MNRAS, 517, 5770
Zheng Z., Ramirez-Ruiz E., 2007, ApJ, 665, 1220
Zhu-Ge J.-M., Luo J.-W., Zhang B., 2022, Machine Learning Classification of Fast Radio Bursts: II. Unsupervised Methods (arXiv:2210.02471), doi:10.48550/arXiv.2210.02471, http://arxiv.org/abs/2210.02471
de Beurs Z. L., Islam N., Gopalan G., Vrtilek S. D., 2022, arXiv e-prints
van Rijsbergen C. J., 1979, Information Retrieval. Butterworth, London

This paper has been typeset from a TEX/LATEX file prepared by the author.